7-24-2008

Extra-large remnant recoil velocities and spins from near-extremal-bowen-york-spin black-hole binaries

Sergio Dain

Carlos Lousto

Yosef Zlochower

Recommended Citation

Extra-Large Remnant Recoil Velocities and Spins from Near-Extremal-Bowen-York-Spin Black-Hole Binaries

Sergio Dain,[1,2] Carlos O. Lousto,[3] and Yosef Zlochower[3]

[1]*Facultad de Matemática, Astronomía y Física, Universidad Nacional de Córdoba,*
Ciudad Universitaria (5000) Córdoba, Argentina.
[2]*Max Planck Institute for Gravitational Physics (Albert Einstein Institute) Am Mühlenberg 1 D-14476 Potsdam Germany.*
[3]*Center for Computational Relativity and Gravitation,*
School of Mathematical Sciences, Rochester Institute of Technology,
78 Lomb Memorial Drive, Rochester, New York 14623
(Dated: July 17, 2008)

We evolve equal-mass, equal-spin black-hole binaries with specific spins of $a/m_H \sim 0.925$, the highest spins simulated thus far and nearly the largest possible for Bowen-York black holes, in a set of configurations with the spins counter-aligned and pointing in the orbital plane, which maximizes the recoil velocities of the merger remnant, as well as a configuration where the two spins point in the same direction as the orbital angular momentum, which maximizes the orbital hang-up effect and remnant spin. The coordinate radii of the individual apparent horizons in these cases are very small and the simulations require very high central resolutions ($h \sim M/320$). We find that these highly spinning holes reach a maximum recoil velocity of ~ 3300 km s^{-1} (the largest simulated so far) and, for the hangup configuration, a remnant spin of $a/m_H \sim 0.922$. These results are consistent with our previous predictions for the maximum recoil velocity of ~ 4000 km s^{-1} and remnant spin; the latter reinforcing the prediction that cosmic censorship is not violated by merging highly-spinning black-hole binaries. We also numerically solve the initial data for, and evolve, a single maximal-Bowen-York-spin black hole, and confirm that the 3-metric has an $\mathcal{O}(r^{-2})$ singularity at the puncture, rather than the usual $\mathcal{O}(r^{-4})$ singularity seen for non-maximal spins.

PACS numbers: 04.25.Dm, 04.25.Nx, 04.30.Db, 04.70.Bw

I. INTRODUCTION

Highly spinning black holes play an important role in astrophysics, from powering active galactic nuclei (AGN), to γ-ray bursts (GRB) and quasars. While the (indirect) observational evidence for the existence of black holes, stellar mass or supermassive, is overwhelming, the actual observational evidence for black-hole spin is scarce. There have been attempts to measure the central black hole spin in AGN [1, 2], Seyfert galaxies [3], and quasars [4]. The x-ray spectra of accretion disks around stellar mass black holes can also provide information about their spins [5, 6, 7].

The recent dramatic breakthroughs in the numerical techniques to evolve black-hole-binary spacetimes [8, 9, 10] has led to rapid advancements in our understanding of black-hole physics. Notable among these advancements are developments in mathematical relativity, including systems of PDEs and gauge choices [11, 12, 13], the exploration of the cosmic censorship [14, 15, 16, 17, 18], and the application of isolated horizon formulae [15, 16, 19, 20, 21, 22]. These breakthroughs have also influenced the development of data analysis techniques through the matching of post-Newtonian to fully-numerical waveforms [23, 24, 25, 26]. In particular, the moving punctures approach proved to work in a wider realm than was originally thought. Notably, it has been successfully applied to many-black-hole spacetimes [27, 28], and to black-hole–neutron star evolutions [29, 30, 31, 32]. Similarly, the recent discovery of very large merger recoil

kicks [33, 34, 35, 36, 37, 38, 39, 40] has had a great impact in the astrophysical community, with several groups now seeking for observational traces of such high speed holes as the byproduct of galaxy collisions [41, 42, 43, 44].

The first study of generic black-hole-binary configurations (i.e. binaries with unequal component masses and spins, and spins not aligned with each other or the orbital angular momentum) was described in Ref. [33], and, based on the results of that study, a semi-empirical formula to estimate the recoil velocities of the remnant black holes was proposed, finding recent confirmation in [35, 45, 46]. The spin contributions to the recoil velocity are generally larger than those due to the unequal masses, and, in particular, the spin component in the orbital plane has the largest effect [33], leading to a maximum recoil velocity of about $3500 - 4000$ km s^{-1} [35]. The recoil velocities acquired by the remnant of the merger of black-hole binaries has many interesting astrophysical consequences [33], particularly since spinning black holes can accelerate the merged hole high enough to eject the remnant from the host galaxy. Recently a quasar, displaying blue shifted emission lines by $2650 \, km/s$ with respect to its host galaxy, has been observed [47].

In all the above simulations, the evolution was started using conformally flat initial data. This choice has the advantage of being easy to implement, with the (apparently) minor drawback of introducing a short, non-physical burst of radiation at the start of the simulation. Apart from this initial burst, there appears to

be no unphysical behavior associated with conformally flat initial data, and this choice remains popular (See Refs. [48, 49] for more astrophysically realistic initial data using post-Newtonian information). The simplest initial data, Bowen-York (BY), gives the extrinsic curvature, K_{ij} analytically by assuming that it is transverse and traceless (See [50] for an alternative prescription). A particularly interesting feature of the conformally flat ansatz for the 3-metric is that these data cannot model maximally rotating Kerr black holes (such holes are not conformally flat in any smooth slice), but have a limiting spin [50, 51] of $S/M_{ADM}^2 \approx 0.928$ for BY data and $S/M_{ADM}^2 \approx 0.932$ for conformally Kerr extrinsic curvature [50]. Here S denotes the spin of the black hole and M_{ADM} the total ADM mass.

The spin of the merger remnant is similarly important both because high-spin black holes are more efficient at converting accreting matter into radiation than lower-spin holes, and because of open questions regarding cosmic censorship. This issues have already been studied in the 'Lazarus' approach to numerical evolutions [52] and in early evolutions using the 'moving punctures' approach [14, 15, 16]. Recently the issue has been revisited in the context of unequal mass holes [17, 18, 53, 54, 55], and highly-elliptical, equal-mass binaries [56, 57]. In the current work we show that, for the maximum possible spin for Bowen-York black holes, the merger remnant will always have sub-maximal spins.

This paper is organized as follows: in Sec. II A we describe the Bowen-York initial data for a single spinning black hole and how one can obtain the maximum possible spin for a Bowen-York black hole, in Sec. II C we describe how we obtain initial data for black-hole binaries with nearly maximal BY spin, in Sec. III we describe the numerical techniques used to evolve these binaries, in Sec. IV we give the results and analysis from the numerical evolutions, and in Sec. V present our conclusions.

II. INITIAL DATA

An *initial data set* for the Einstein vacuum equations is given by a triple $(\mathcal{M}, \gamma_{ij}, K_{ij})$ where $\mathcal{M}$ is a connected 3-dimensional manifold, γ_{ij} a (positive definite) Riemannian metric, and K_{ij} a symmetric tensor field on $\mathcal{M}$, such that the constraint equations

$$D_j K^{ij} - D^i K = J^i, \tag{1}$$
$$R - K_{ij}K^{ij} + K^2 = 2\mu, \tag{2}$$

are satisfied on $\mathcal{M}$. Where D and R are the Levi-Civita connection and the Ricci scalar associated with γ_{ij}, and $K = K_{ij}\gamma^{ij}$. The vector J^i and the scalar function μ are determined by the stress energy tensor of the sources which describes the matter content of the spacetime. In these equations the indices are moved with the metric γ_{ij} and its inverse γ^{ij}.

A. Maximum Spin Bowen-York initial data

The Bowen-York family of initial sets [58] represents a relevant class of data suitable for numerical simulations of black-hole binaries. They are constructed using the conformal method for solving the constraint equations (1)–(2) (for a recent review on this method see [59] and references therein). Let us consider one member of this family, namely the spinning Bowen-York data. These data describe a (non-stationary) black hole with intrinsic angular momentum. In order to construct the data we prescribe $\tilde{K}^{ij}$, a symmetric, trace free and divergence free tensor with respect to the flat metric δ_{ij}

$$\tilde{K}^{ij} = \frac{6}{r^3} n^{(i}\epsilon^{j)kl}S_k n_l, \tag{3}$$

where r is the spherical radius, n^i the corresponding radial unit normal vector, ϵ^{ijk} the flat volume element and S_k an arbitrary constant vector which will give the total spin of the data. In this equation the indices are moved with the flat metric δ_{ij}. The data are given by

$$\gamma_{ij} = \varphi^4 \delta_{ij} \quad K^{ij} = \varphi^{-10}\tilde{K}^{ij}, \tag{4}$$

where the conformal factor satisfies the following equation (which is the conformal version of the Hamiltonian constraint (2))

$$\Delta\varphi = -\frac{18S^2 \sin^2\theta}{8r^6\varphi^7}. \tag{5}$$

where $S^2 = S_i S_j \delta^{ij}$ and Δ is the flat Laplacian.

For any solution φ of Eq. (5) the metric γ_{ij} and K_{ij} given by (4) define a solution of the vacuum (i.e. $J^i = \mu = 0$) constraint equations (1)–(2). In order to find a unique and physically relevant solution of (5) we need to impose appropriate boundary conditions for φ. This is essentially equivalent to prescribe the manifold $\mathcal{M}$ of the initial data. For example, Eq. (5) is singular at $r = 0$, it follows that the solution φ can not be regular at $r = 0$ and hence the origin can not be in the manifold $\mathcal{M}$. That is $\mathbb{R}^3$ is not allowed as manifold in this class of initial data. In the present case the manifold will be $\mathcal{M} = \mathbb{R}^3 \setminus \{0\}$, the origin $r = 0$ represents another end of the initial data.

Boundary conditions for black holes are prescribed as follows. Let $m^p > 0$ be an arbitrary number. Define the function u by

$$\varphi = 1 + \frac{m^p}{2r} + u. \tag{6}$$

Using (5) we obtain an equation for u outside the origin

$$\Delta u = -\frac{18rS^2 \sin^2\theta}{8(r + \frac{m^p}{2} + ru)^7}. \tag{7}$$

If u is positive (this will be the case as a consequence of the maximum principle) then the denominator of Eq. (7) never vanishes and hence this equation is regular at the

origin. The idea is to impose this equation also at the origin, that is, we want to solve (7) in $\mathbb{R}^3$ with a boundary condition at infinity

$$\lim_{r \to \infty} u = 0. \qquad (8)$$

It is well known that for each $m^p > 0$ there exists a unique solution u of (7) which satisfies the boundary condition (8). The solution is positive and from standard elliptic theory it follows that it is smooth outside the origin and it is C^2 at the origin (this loss of differentiability is due to the presence of the function r on the right hand side of Eq. (7) which is not smooth at the origin). This is what in the numerical relativity is called the puncture method [60], the parameter m^p is called the mass parameter of the puncture. By Eq. (6), the singular part of φ at $r = 0$ is $\mathcal{O}(1/r)$, this implies that the physical fields γ_{ij}, K_{ij} are asymptotically flat at the end $r = 0$.

The physical parameters of the data are given by S which represent the angular momentum of the data and the total ADM mass M_{ADM}, which is given by the following formula

$$M_{ADM} = m^p + m_u, \qquad (9)$$

where m_u is the coefficient $\mathcal{O}(1/r)$ of u, that is

$$u = \frac{m_u}{2r} + \mathcal{O}(1/r^2) \qquad (10)$$

as $r \to \infty$. Note that in order to calculate the total mass M_{ADM} we need to solve the non-linear equation (7)

The solution u depends on the coordinates x and the two parameters m^p and S. However, there exists a scale invariance for equation (7). Namely, if we have a solution $u(m^p, S, x)$, for parameters S and m^p, then the rescaled function $u(\lambda m^p, \lambda^2 S, \lambda x)$, where λ is an arbitrary positive number, is also a solution. This means that the solution depends non trivially only on one parameter. We chose to fix S and vary m^p. Note that the following quotient is scale invariant

$$\epsilon_S = \frac{S}{M_{ADM}^2}. \qquad (11)$$

For a Kerr black hole we have $\epsilon_S \leq 1$ and $\epsilon_S = 1$ implies that the black hole is extreme. For general axially symmetric vacuum black holes (which in particular includes the spinning Bowen-York data) we also have $\epsilon_S \leq 1$ [61][62] and $\epsilon_S = 1$ if and only if the data are slices of extreme Kerr black hole. Since the Bowen-York data are not slices of the extreme Kerr black hole it follows that $\epsilon_S < 1$ for this family. What is the maximum value for ϵ_S in this family? This question was explored numerically in [50, 51, 63]. In these references it was observed that in the limit $S \to \infty$ (for fixed m^p) the ratio ϵ_S reach an asymptotic maximum value. Because of the scaled invariance mentioned above this limit is equivalent to $m^p \to 0$, with S fixed. What was not clear at all is

that in fact in the limit we get a well behaved solution of the constraint equation. This is precisely the question we want to answer here. That is, we want to give numerical evidence that the limit

$$u(S, x) = \lim_{m^p \to 0} u(m^p, S, x) \qquad (12)$$

exists and defines a solution of the constraint equations. An analytical proof of this is detailed in [64]. We will call this new solution the extreme Bowen-York spinning data because it has the maximum amount of angular momentum per mass in this family [92].

In the limit $m^p \to 0$ the difference between φ and u is just a constant and Eq. (7) become singular at the origin, hence the limit solution u can not be regular at the origin. If we assume that $u = \mathcal{O}(r^\alpha)$ at $r = 0$ for some real number α, using Eq. (7) we get that $\alpha = -1/2$. That is, we expect the following behavior at the origin

$$u = \mathcal{O}\left(\frac{1}{\sqrt{r}}\right). \qquad (13)$$

This behavior is confirmed by the numerical simulations presented in the next subsection II B.

We have seen that the limit solution u has a different fall off behavior at the origin than the family $u(m^p)$ for $m^p > 0$, in particular the conformal factor for $m^p > 0$ behaves like $\mathcal{O}(1/r)$ at $r = 0$ but in the limit $m^p \to 0$ it behaves like $\mathcal{O}(1/\sqrt{r})$. This implies a change in the fall off behavior off the physical fields at the end $r = 0$. This end will not be asymptotically flat in the extreme limit.

We illustrate the same phenomena with two important examples. The first one is the Reissner-Nordström black hole initial data. In isotropic coordinates, a canonical slice $t = $ const for the Reissner-Nordström black hole spacetime with mass M_{ADM} and charge q (for a black hole we always have $q \leq M_{ADM}$) defines the following initial data set

$$\gamma_{ij} = \varphi^4 \delta_{ij}, \quad K^{ij} = 0, \quad J^i = 0, \quad \mu = \frac{q^2}{r^4 \varphi^8}, \qquad (14)$$

where the conformal factor is given by

$$\varphi = \frac{1}{2r} \sqrt{(q + 2r + M_{ADM})(-q + 2r + M_{ADM})}. \qquad (15)$$

The conformal factor satisfies the following equation (analog to Eq. (5))

$$\Delta \varphi = -\frac{q^2}{4r^4 \varphi^3}. \qquad (16)$$

For this solution define the parameter

$$m^p = \sqrt{M_{ADM}^2 - q^2}, \qquad (17)$$

and the function u by

$$u = \varphi - 1 - \frac{m^p}{2r}. \qquad (18)$$

For $m^p > 0$, the function u is bounded at $r = 0$. The extreme limit $q \to M_{ADM}$ corresponds to $m^p \to 0$. In this limit we have

$$\varphi = \sqrt{\frac{M_{ADM}}{r} + 1}, \quad u = \varphi - 1, \qquad (19)$$

and hence $\varphi = u = \mathcal{O}(1/\sqrt{r})$. Note that although Eq. (16) is different from (5), the powers of r and φ on the right hand side are such that if we assume $u = \mathcal{O}(r^\alpha)$ at $r = 0$ we get $\alpha = -1/2$ as in the Bowen-York spinning black hole.

The second example is given by the Kerr black hole initial data in quasi-isotropic coordinates. Let S and M_{ADM} be the total angular momentum and mass of the Kerr spacetime. Define the parameter m^p by

$$m^p = \sqrt{M_{ADM}^2 - a^2}, \quad a = \frac{S}{M_{ADM}^2}. \qquad (20)$$

As in the previous example, the extreme limit $\sqrt{S} \to M_{ADM}$ of Kerr metric correspond $m^p \to 0$. The explicit expression of these data can be found in [65], in this reference it is proved that the conformal factor behaves in a similar way as the Reissner-Nordström in the limit $m^p \to 0$. For completeness, we reproduce this calculation and adapt it to our setting. We use the coordinate transformation [66]

$$r = \bar{r}\left(1 + \frac{m + a}{2\bar{r}}\right)\left(1 + \frac{m - a}{2\bar{r}}\right), \qquad (21)$$

where r is the standard Boyer-Lindquist radial coordinate, which puts the Kerr metric in the quasi-isotropic form

$$ds^2 = \phi_K^4\left[e^{-2q_K}\left(d\bar{r}^2 + \bar{r}^2 d\theta^2\right) + \bar{r}^2\sin\theta^2 d\phi^2\right], \qquad (22)$$

where ds^2 is the spatial line element,

$$e^{-2q_K} = \frac{r^2 + a^2\cos^2\theta}{r^2 + a^2 + \frac{2ma^2r\sin^2\theta}{r^2 + a^2\cos^2\theta}}, \qquad (23)$$

and

$$\phi_K^4 = \bar{r}^{-2}\left[r^2 + a^2 + \frac{2ma^2r\sin^2\theta}{r^2 + a^2\cos^2\theta}\right]. \qquad (24)$$

The function ϕ^4 has the expansion

$$\phi_K^4 = \frac{\left(a^2 - m^2\right)^2}{16\bar{r}^4} + \frac{m^3 - a^2m}{2\bar{r}^3} + \frac{a^2 + 3m^2}{2\bar{r}^2} + \qquad (25)$$

$$\frac{2m\left(-2\cos(2\theta)a^2 + a^2 + m^2\right)}{\left(m^2 - a^2\right)\bar{r}} + \mathcal{O}(1) \qquad (26)$$

when $a < m$. However, for $a = m$ expansion (25) is singular. In this case ϕ^4 has the form:

$$\phi_K^4 = \frac{4m(m + \bar{r})\left(2m^2 + 2\bar{r}m + \bar{r}^2\right)}{\bar{r}^2\left(\cos(2\theta)m^2 + 3m^2 + 4\bar{r}m + 2\bar{r}^2\right)} + 1, \qquad (27)$$

which has the expansion

$$\phi_K^4 = \frac{8m^2}{(\cos(2\theta) + 3)\bar{r}^2} + \frac{32m\cos^2(\theta)}{(\cos(2\theta) + 3)^2\bar{r}} + \mathcal{O}(1). \qquad (28)$$

Thus the behavior of ϕ_K changes from

$$\phi_K \sim \sqrt{a^2 - m^2}/(2\bar{r}) + \mathcal{O}(1)$$

to

$$\phi_K \sim \frac{\sqrt{2m/\bar{r}}}{\sqrt[4]{1 + \cos^2\theta}} + \mathcal{O}(r^{1/2})$$

in the extremal case $a = m$ (the horizon is then mapped to the limiting surface $\bar{r} = 0$). Hence, just as in the maximal Bowen-York case, the $\bar{r} = 0$ coordinate singularity corresponds to an end which is not asymptotically flat.

B. Numerical Test of Highly-Spinning BY Initial Data

We first solve the initial data for one black hole presented in section II A. We used a modified version of BAM_Elliptic thorn [60, 67] in order to solve for the case where $S/M^2 = 1$ (here M denote an scale factor) and $m^p = 0$ on a uniform grid with resolution $h = 0.0035M$ and outer boundary at $0.64M$ (here we are only interested in the singular behavior, which is not affected by inaccurate boundary data). In order to avoid the singularity itself, we constructed the grid such that the origin was located halfway between gridpoints. We fit γ_{xx} along the lines $y = z = h/2$ and $x = y = h/2$ to the form: $\gamma_{xx} = a + b/(x^2 + 2c^2)$ (with a similar form for z) and perform a non-linear least-squares fit (See Fig. 1). We find that $\gamma_{xx}(x) = 11.483 + 2.5042/(x^2 + 2(0.00231057)^2$ and $\gamma_{xx}(z) = 265.319 + 1.91325/(x^2 + 2(0.00192925)^2)$. Note that the c parameter differs from the expected $h/2$ but this functional form captures the expected singular behavior to high accuracy. In Fig. 2 we plot the function u for various choices of mass parameter m_p for a configuration consisting of two black holes, one at the origin and one at $x = -20M$, with the former hole having spin $S/M^2 = 1$ and the latter nonspinning. From the plot one can see that, although u is finite, u ends to $1/\sqrt{r}$ as m_p tends to zero.

We are not able to calculate the ADM mass M_{ADM} of the data, because we needed very high resolution near the puncture $r = 0$, leaving too few point outside the horizon. Instead, we compute the horizon mass m_H given by $m_H = \sqrt{m_{irr}^2 + S^2/(4m_{irr}^2)}$ where m_{irr} is the irreducible mass (it is expected for these kind of data that $m_H \leq M_{ADM}$, there exists however no proof of this conjecture). Analogous to the ratio (11) we define the quasi local ratio a/m_H, where $a = S/m_H$. For these data the maximum possible value of this quantity is given by $a/m_H \sim 0.93$ [50, 68].

Even the horizon mass m_H is difficult to resolve at the initial surface (the horizon is located at only one point

FIG. 1: The γ_{xx} component of the metric on the initial slice for a single spinning, non-boosted black hole located at the origin with $S = 1M^2$ and the puncture mass parameter $m^p = 0$. Here we plot γ_{xx} versus x ($y = z = .00175M$) and z ($x = y = 0.00175M$) and fits to $\gamma_{xx} = a + b/(x^2 + 2c^2)$ (with a similar form for z). Note that $\gamma_{xx} \propto 1/r^2$ is consistent with the expected $\varphi \propto 1/\sqrt{r}$.
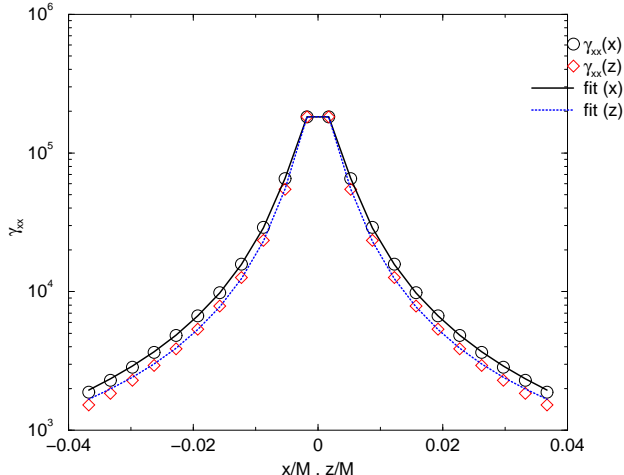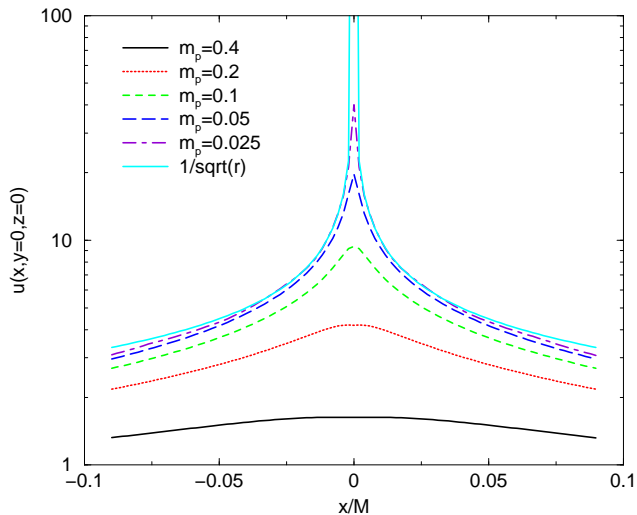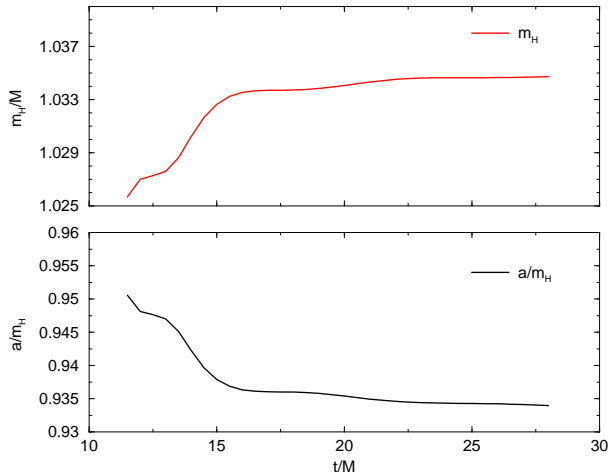

FIG. 3: The horizon mass and specific spin for a maximal BY black hole. Here $S = 1M^2$ and $m^p = 0$. Note that the spin drops rapidly to about $a/m_H = 0.934$ (and is still dropping) after the hole absorbs significant mass. The expected asymptotic value is $a/m_H = 0.928$.

FIG. 2: The function u for finite m_p in the neighborhood of the puncture. Here the data consists of two BH (the second BH is located at $x/M = -20$ and is not shown). The BH at the origin has spin parameter $S/M^2 = 1$. Note that u approaches $1/\sqrt{r}$ as m_p tends to zero.

lution presented in Fig. 3.

In order to measure the horizon mass and the quotient a/m_H in this case, we performed a second unigrid run, this time using fisheye [69, 70], with a central resolution of $h = M/64$ and outer boundaries at $65M$. Initially the horizon has a coordinate radius of zero (akin to extreme Kerr in quasi-isotropic coordinates) that grows to $r \sim 0.3M$ at $t = 15M$ as it absorbs the spurious radiation produced by the conformally flat initial data. In Fig. 3 we show the horizon mass and specific quotient for this run. Note the rapid drop off in the ratio a/m_H between $t = 10M$ and $t = 15$. Due to the relatively poor resolution of this run, and the short evolution time, it is not clear if it asymptotes to $a/m_H = 0.933$, or will continue to drop to the numerically predicted value of 0.928.

C. Spinning-black-hole-binary initial data

The initial data techniques of Sec. II A can be extended to multiple spinning black holes with linear momentum [60]. Here too the 3-metric on the initial slice has the form $\gamma_{ab} = (\psi_{BL} + u)^4 \delta_{ab}$, where ψ_{BL} is the Brill-Lindquist conformal factor, δ_{ab} is the Euclidean metric, and u is (at least) C^2 on the punctures. The Brill-Lindquist conformal factor is given by $\psi_{BL} = 1 + \sum_{i=1} m^p_{[i]}/(2|\vec{r} - \vec{r}_{[i]}|)$, where the sum is over all punctures, $m^p_{[i]}$ is the mass parameter of puncture i ($m^p_{[i]}$ is *not* the horizon mass associated with puncture i), and $\vec{r}_{[i]}$ is the coordinate location of puncture i (we use the notation $[i]$ to distinguish the puncture label from the tensor indices in the equations below). The extrinsic curvature K_{ab} is given by the Bowen-York (BY) ansatz [58]

$r = 0$), we need to perform the evolution of the data to compute it at later times.

These data have axial symmetry and then the spin is a conserved quantity. One part of the radiation emitted by the data will fall into the black hole increasing its area and the other part will scape to infinity. Hence the ratio a/m_H will monotonically decrease during the evolution. This is precisely what we observed in the numerical evo-
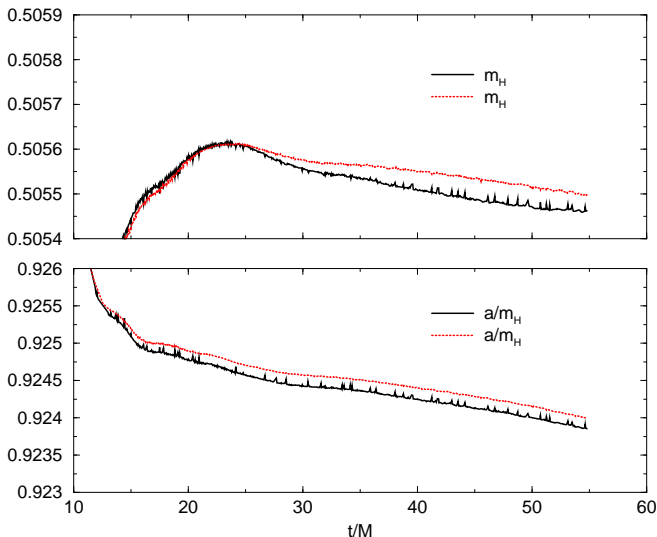
FIG. 4: The specific spins and horizon masses for a binary containing nearly maximal BY spinning holes. The initial spins of the two holes are $a/m_H = 0.967$. The individual horizon masses increase rapidly near $t \sim 15M$ as the black holes absorb the spurious radiation. The spin drops to $a/m_H = 0.924$ since the spurious radiation does not increase the angular momentum of the holes.

and has the form $K^{ab} = \varphi^{-10}\tilde{K}^{ab}$, where

$$\tilde{K}^{ab} = \sum_i \frac{3}{2|\vec{r} - \vec{r}_{[i]}|^2}(2P_{[i]}^{(a}n_{[i]}^{b)} - (\delta^{ab} - n_{[i]}^a n_{[i]}^b)P_i^c n_{[i]c})$$
$$+ \frac{3}{|\vec{r} - \vec{r}_{[i]}|^3}(2S_{[i]c}n_{[i]d}\epsilon^{cd(a}n_{[i]}^{b)}), \quad (29)$$

$\varphi = \psi_{BL} + u$, $\vec{n}_{[i]} = (\vec{r} - \vec{r}_{[i]})/|\vec{r} - \vec{r}_{[i]}|$, and $\vec{P}_{[i]}$ and $\vec{S}_{[i]}$ are the linear and angular momenta of puncture i. As shown in Sec. II A, for a single puncture, if $m^p = 0$, $\vec{P} = 0$, and $\vec{S} \neq 0$ then u is no longer finite at the puncture location, but has a $1/\sqrt{r}$ singularity. Under these conditions, the resulting black hole will have the maximum possible specific spin for Bowen-York type data.

We compute and evolve the black-hole-binary data described above. The ratio a/m_H is a quasi local quantity which is well defined for individual black holes in a binary system (in contrast with the ratio ϵ_S in which appears the ADM mass which is a global quantity). We can obtain specific ratios a/m_H nearly equal to the maximum allowed for BY holes by setting m^p sufficiently small. For the runs presented below we use the puncture approach [60] along with the TwoPunctures [71] thorn to compute initial data for black-hole-binaries. In Fig. 4 we show the isolated horizon spin for the individual holes in a near maximally spinning BY binary (configuration MR0 described below). Note that the spins drop significantly within $10M$ – $20M$ of evolution.

III. NUMERICAL TECHNIQUES

We evolve the black-hole-binary data-sets using the LazEv [9, 72] implementation of the moving puncture approach [9, 10]. In our version of the moving puncture approach we replace the BSSN [73, 74, 75] conformal exponent ϕ, which has logarithmic singularities at the punctures, with the initially C^4 field $\chi = \exp(-4\phi)$. This new variable, along with the other BSSN variables, will remain finite provided that one uses a suitable choice for the gauge. An alternative approach uses standard finite differencing of ϕ [10].

We use the Carpet [76] mesh refinement driver to provide a 'moving boxes' style mesh refinement. In this approach refined grids of fixed size are arranged about the coordinate centers of both holes. The Carpet code then moves these fine grids about the computational domain by following the trajectories of the two black holes.

We obtain accurate, convergent waveforms and horizon parameters by evolving this system in conjunction with a modified 1+log lapse and a modified Gamma-driver shift condition [9, 77], and an initial lapse $\alpha(t = 0) = 2/(1 + \psi_{BL}^4)$. The lapse and shift are evolved with

$$(\partial_t - \beta^i \partial_i)\alpha = -2\alpha K \quad (30a)$$
$$\partial_t \beta^a = B^a \quad (30b)$$
$$\partial_t B^a = 3/4\partial_t\tilde{\Gamma}^a - \eta B^a. \quad (30c)$$

These gauge conditions require careful treatment of χ, the inverse of the three-metric conformal factor, near the puncture in order for the system to remain stable [9, 70, 78]. In Ref. [12] it was shown that this choice of gauge leads to a strongly hyperbolic evolution system provided that the shift does not become too large.

We use AHFinderDirect [79] to locate apparent horizons. We measure the magnitude of the horizon spin using the Isolated Horizon [15, 16, 19, 20, 21, 22] algorithm detailed in [80]. This algorithm is based on finding an approximate rotational Killing vector (i.e. an approximate rotational symmetry) on the horizon, and given this approximate Killing vector ξ^a, the spin magnitude is

$$S_{[\xi]} = \frac{1}{8\pi}\oint_{AH}(\xi^a R^b K_{ab})d^2V \quad (31)$$

where K_{ab} is the extrinsic curvature of the 3D-slice, d^2V is the natural volume element intrinsic to the horizon, and R^a is the outward pointing unit vector normal to the horizon on the 3D-slice. We measure the direction of the spin by finding the coordinate line joining the poles of this Killing vector field using the technique introduced in [16]. Our algorithm for finding the poles of the Killing vector field has an accuracy of $\sim 2°$ (see [16] for details).

We measure radiated energy, linear momentum, and angular momentum, in terms of ψ_4, using the formulae provided in Refs. [81, 82]. However, rather than using the full ψ_4 we decompose it into ℓ and m modes and solve for the radiated linear momentum, dropping terms

TABLE I: Initial data parameters for the maximum recoil configurations MR0 – MR315 and the maximum hangup configuration MH. For MR0 – MR315 the punctures are located at $\vec{x}/M = (\pm 3.564036838, 0, 0)$, with momenta $\vec{p}/M = (0, \pm 0.1254868859, 0)$ and spins $\vec{S} = \pm(S_x, S_y, 0)$. In all cases the orbital frequency is $M\omega = 0.045$ and the puncture mass parameters are $m^p/M = 0.08967$. For MH the punctures are located at $\vec{X}/M = (\pm 4.083304018, 0, 0)$, with momenta $\vec{P} = (0, \pm 0.1046285561, 0)$ and spin $\vec{S}/M^2 = +(0, 0, 0.2362330001)$. The orbital frequency is $M\omega = 0.035$ and the puncture mass parameters are $m^p/M = 0.107949$.

Config	M_{ADM}	S_x/M^2	S_y/M^2
MR0	1.000000	0	0.23642497
MR45	0.999493	−0.16717770	0.16717770
MR90	0.998982	−0.23642497	0
MR135	0.999493	−0.16717770	−0.16717770
MR180	1.000000	0	−0.23642497
MR225	0.999493	0.16717770	−0.16717770
MR270	0.998982	0.23642497	0
MR315	0.999493	0.16717770	0.16717770
MH	1.000000		

with $\ell \geq 5$. The formulae in Refs. [81, 82] are valid at $r = \infty$. We obtain highly accurate values for these quantities by solving for them on spheres of finite radius (typically $r/M = 25, 30, 35, 40$), fitting the results to a polynomial dependence in $l = 1/r$, and extrapolating to $l = 0$. We perform fits based on a linear and quadratic dependence on l, and take the final values to be the average of these two extrapolations with the differences being the extrapolation error.

IV. RESULTS

Evolving black holes with specific spins of $a/m_H \sim 0.92$ is challenging because the horizons appear quite small. In our coordinates, the initial horizon radii were $0.04M$. We evolved these data using 14 levels of refinement with a finest resolution of $h = M/320$ (the highest resolution reported so far in numerical simulations of binary black holes). The outer boundaries were located at $\pm 640M$ in all directions and the resolution on the coarsest grid was $h = 12.8M$. We obtained the spin, position, and momentum parameters of the initial data using third-order post-Newtonian parameters for equal-mass quasi-circular binaries with spins aligned with the linear momentum of the two holes, and aligned with the orbital angular momentum. In all cases we took the spin of the two holes to be $a/m_H = 0.92$. We set the puncture mass parameters of the two holes such that the total ADM mass was 1M. The initial data parameters are summarized in Table I. Note that we normalize the MR0 configuration to ADM mass of 1M, but keep the same mass parameters when we rotate the spin. Hence MR45 – MR315 have slightly different ADM masses.

FIG. 5: The xy projections of the puncture trajectories for MR0 and MR45, the latter rotated by an angle Θ_{cor} so that the late inspiral and merger phases overlap.
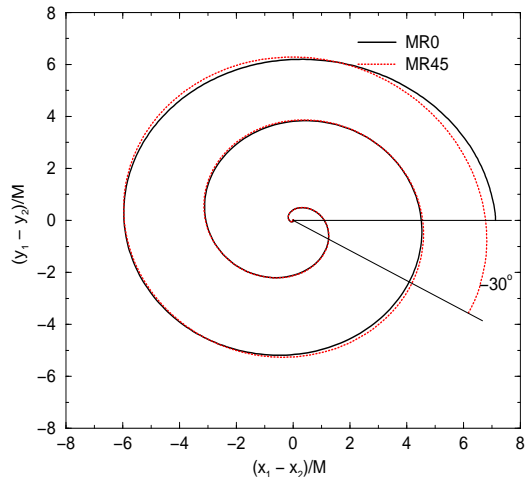
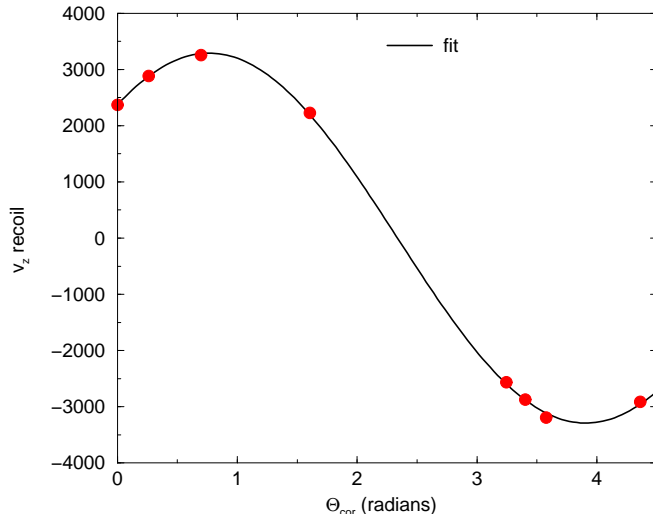## A. Large Recoil Velocities

In Ref. [33] we proposed a semi-empirical formulae for the dependence of the merger recoil velocity on the spins and mass ratio of the two black holes in a binary. Our formula predicts that the largest recoils occur for two equal-mass, equal-spin black holes with spins pointing in the orbital plane and counter aligned with each other. In this configuration the recoil is proportional to the spin-amplitude and varies sinusoidally with the angle between the direction of the spins at merger and the linear momentum direction. The resulting recoil will be perpendicular to the orbital plane. We were able to test this prediction [35] by evolving a binary with spins $a/m_H = 0.5$ (initially pointing in the direction of the linear momentum) and then evolving a set of binary configuration with the same orbital parameter, but with the initial spin directions rotated by an angle Θ. We found that we could fit the resulting recoil velocities to a $\cos(\Theta - \Theta_0)$ dependence to high accuracy. Implicit in this approach is that the angle between the spins and linear momentum at merger is given by the angle at merger for the $\Theta = 0$ configuration plus Θ. This, in turn, requires that the xy projection of the trajectories be independent of Θ.

Unlike in Ref. [35], here we found for the MR0 — MR315 configurations that rotating the initial spin direction alters the xy-projection of the trajectories by introducing varying ellipticity to the orbit and possibly due to spin-orbit coupling. However, after rotating the xy-projected trajectories for M45 – M315 by an angle Θ_{rot} (See Fig. 5, and Ref. [83] for a description of the technique), we found that they overlap for the late inspiral and plunge with projected MR0 trajectory. We then take the initial spin orientation, plus this trajectory rotation, as the angle between MR45 – MR315 spin direction at merger with the MR0 spin direction at merger. We then fit the z-component of the recoil versus this angle. The

TABLE II: Recoil velocity (in the z-direction) for the MR0—MR315 configuration, initial angle Θ_{con} between the spin directions of the MR45—MR315 and MR0, and (approximate) angle Θ_{cor} between spin directions of MR45—MR315 and MR0 at merger. Here $\Theta_{cor} = \Theta_{con} + \Theta_{rot}$.

Config	Θ_{con}	Θ_{cor}	$V_z(\text{km s}^{-1})$
MR0	$0°$	$0°$	2372 ± 12
MR45	$45°$	$15°$	2887 ± 27
MR90	$90°$	$40°$	3254 ± 19
MR135	$135°$	$92°$	2226 ± 6
MR180	$180°$	$186°$	-2563 ± 8
MR225	$225°$	$195°$	-2873 ± 23
MR270	$270°$	$205°$	-3193 ± 45
MR315	$315°$	$250°$	-2910 ± 1

FIG. 6: Recoil velocity versus corrected rotation angle for the MR0—MR315 configurations and a non-linear least-squares fit to a simple sinusoidal behavior. Note that the corrected rotation angles are not distributed uniformly in the range $(0, 2\pi)$.

results are summarized in Table II and Fig. 6 (with several runs having significantly higher recoil velocities than any previous simulation). A fit of v_z versus Θ_{cor} (where Θ_{cor} is the corrected angle between MR45 – MR315) and MR0 gives: $v_z(\text{km s}^{-1}) = 3290.14 \cos(\Theta_{cor} - 0.765885)$ where Θ_{cor} is measured in radians and the confidence interval for the amplitude is $(3243, 3337)$. Our empirical formula predicts an amplitude of 3461 ± 58. These results are with $2.3\,\sigma$ of the prediction for $a/m_H = 0.923$. A relatively large error is not unexpected due to the difficulty in evolving systems with such small scale features and the ellipticity introduced by the spurious radiation. On the other hand, this may also indicate a non-linear (in a/m_H) term is present that reduces the maximum possible recoil.

FIG. 7: The puncture trajectories and first common apparent horizon for the MH configuration. Note that the binary completes ~ 7.5 orbits prior to merger.
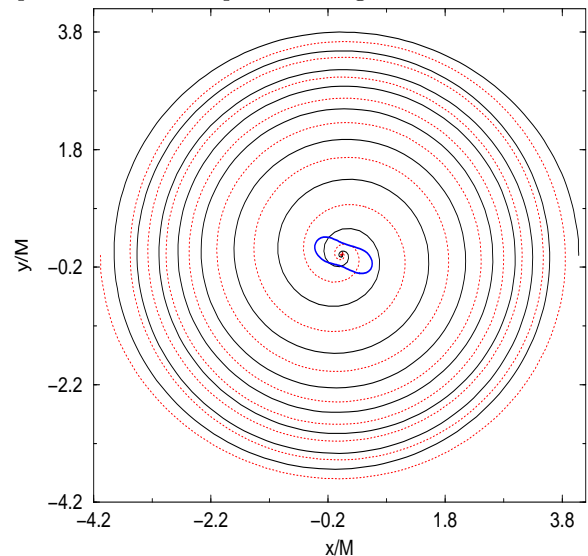
B. Orbital Hangup

Of particular interest is the spin-orbit hangup effect [14, 17, 84] when the two spins are aligned with the orbital angular momentum. Here we examine configuration MH, where the two spins have near maximal (for BY data) spins. We evolved configuration MH with 14 levels of refinement, maximum resolution of $h = M/320$, and outer boundaries at $1281M$. In Fig. 7 we show the xy trajectories of the punctures as well as the first common apparent horizon. Note that the binary completes ~ 7.5 orbits before the first common apparent horizon forms. In Fig. 8 we show $r = |\vec{r}_1 - \vec{r}_2|$ (where $\vec{r}_i$ is the location of puncture i) versus orbital phase ϕ_{orbit}. The initial eccentricity, as is evident by the oscillation in $r(\phi_{orbit})$, damp with time. The hangup effect is clearly seen in Fig. 9, which shows the xy projections of the trajectory difference $\vec{r}_1 - \vec{r}_2$ for the MH and MR0 configurations. In Fig. 10 we show the real part of the $(\ell = 2, m = 2)$ mode of ψ_4 for the MH configuration. We measure the remnant mass and spin three different ways: from the isolated horizon formalism, from the radiated energy and angular momentum, and from the quasi-normal decay of the late-time waveform. Results for the isolated horizon calculation were affected by late-time boundary effects due to relatively poor resolution in the outer zones. The results are summarized in Table III. To calculate the horizon mass and spin from the quasi-normal modes we used the results of [85] and a fit to $\exp(-t/\tau)\sin(\omega t - \theta_0)$ for the real and imaginary parts of the $(\ell = 2, m = 2)$ mode of ψ_4 at $r = 40M$. We found $\tau/M = 15.097 \pm .0074$ and $M\omega = 0.76579 \pm 0.00006$ (the errors reported are the differences in τ and ω for the real and imaginary parts of ψ_4). We also calculated the remnant mass and spin from

FIG. 8: The puncture separation, and first derivative (see inset), versus orbital phase for the MH configuration. Note the decaying oscillations that indicate the ellipticity is significantly reduced after 2 orbits.
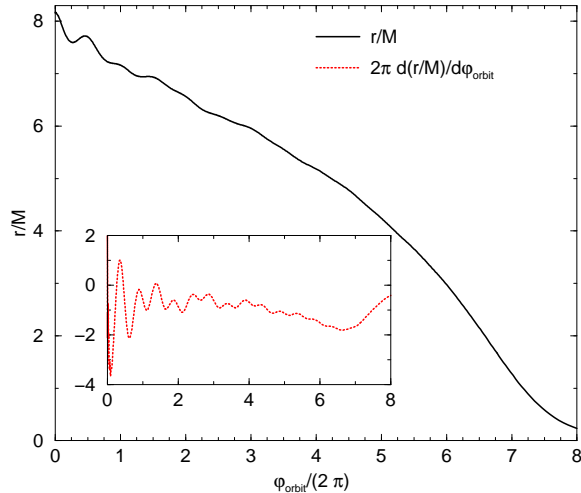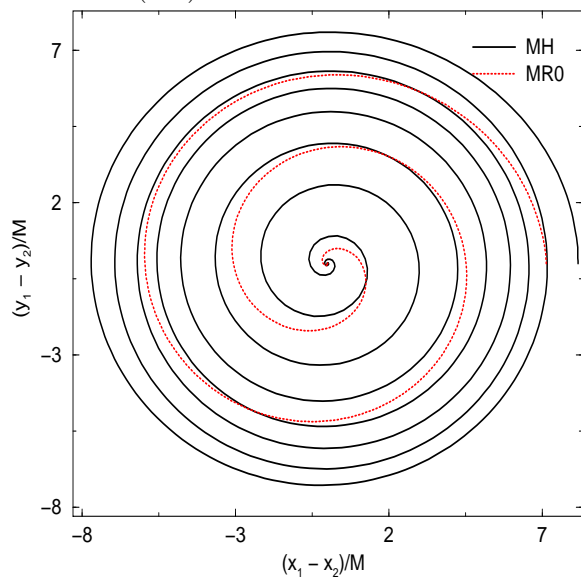

FIG. 9: The xy projection of the trajectory difference $\vec{r}_1 - \vec{r}_2$ for the MH and MR0 configurations. Note the significant hangup effect when the spins are parallel to the orbital angular momentum (MH).

FIG. 10: The real part of the ($\ell = 2, m = 2$) mode of ψ_4 for the MH configuration showing the orbital dynamics and quasi-normal decay.
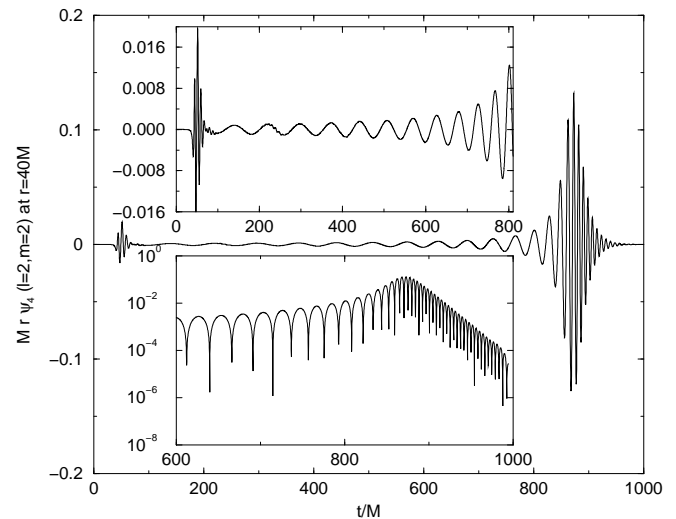

TABLE III: Remnant horizon mass and spin for configuration MH based on the isolated horizon (IH) calculation, the radiated energy and angular momentum, and the quasi-normal frequency (QNM).

	IH	Radiation	QNM
m_H	0.9095 ± 0.0005	0.9162 ± 0.0024	0.9146 ± 0.0002
a/m_H	0.922 ± 0.001	0.928 ± 0.015	0.922 ± 0.001

V. CONCLUSION

We have evolved equal-mass, equal-spin black-hole-binary configuration with nearly maximal BY spin of $a/m_H = 0.923$, the highest spins simulated thus far, both for spins pointing in the same direction as the orbital angular momentum and for spins (counter-aligned) pointing in the orbital plane. In the former case we see a significant orbital hangup (for seven orbits prior to merger), and confirmed that the remnant spin is non-maximal and agrees with our previous predictions based on a least-squares fit of remnant spin versus initial spin [14, 15, 16, 86]. While in latter case we find that the maximum recoil is $v_{\rm recoil} = 3290 \pm 47$ km s^{-1}, in qualitative agreement with our prediction of 3461 ± 58 km s^{-1}. The deviation of our measured recoil velocity from the predicted value is likely due to the relatively poor effective resolution (i.e. the number of gridpoints across the initial horizons), as well as eccentricities introduced by the significant amount of spurious radiation or non-linear corrections to the kicks formula. We have confirmed the sinusoidal dependence of the recoil on the initial spin direction and that the recoil varies essentially linearly with the magnitude of the spin for a fixed initial spin direction. Note that the measured recoil of

the radiated energy and angular momentum. Here too, inaccuracies due to relatively poor resolution in the outer zones affect the calculation. For all three methods, the final spin is in qualitative agreement with the prediction of $a/m_H = 0.928$ in [14, 15], but differs from the prediction $a/m_H = 0.9400 \pm 0.0019$ in [53] for initial specific spins of 0.92.

$v_{\mathrm{recoil}} = 3254 \pm 19$ km s^{-1} for the MR90 configuration is the largest recoil velocity measured for an actual simulation to-date, and would expel the BH remnant from any known galaxy.

All our numerical calculations confirm cosmic censorship. In particular, highly spinning black holes, which are close to the extreme Kerr limit, do not develop naked singularities. Moreover, the system always decays asymptotically in time to a final black hole which satisfy the inequality between mass and spin of the Kerr black hole.

There is a curious analogous behavior between the conformal factor of the extreme spinning BY initial data as $r \to 0$, i.e. $\varphi \sim 1/\sqrt{r}$, and the late-time behavior of the determinant of the 3-metric for a Schwarzschild black hole [87, 88, 89, 90] with the standard moving-puncture choice for the gauge Eqs. (30). Here $r = 0$ corresponds to the horizon on the initial slice, which has finite surface area, while in the case of Schwarzschild, if we take the limit $t \to \infty$ and then $r \to 0$, we approach a sphere of finite surface area inside the horizon. It seems that, as we increase the spin of the black hole to its maximum allowed value, we find a new, extreme solution that has a different behavior from the non-extreme cases ($1/r$

vs. $1/\sqrt{r}$). The limit of stationarity, for $t \to \infty$ of submaximal data, also leads to a new behavior for the conformal factor $\phi \sim 1/\sqrt{r}$, not present at finite time. In both cases the data transition from a slicing that contains two asymptotically flat ends to one that contains one asymptotically flat end and one cylindrical end.

[1] C. S. Reynolds, L. W. Brenneman, and D. Garofalo, Astrophys. Space Sci. **300**, 71 (2005), astro-ph/0410116.

[2] G. Lodato and J. E. Pringle, Mon. Not. Roy. Astron. Soc. **368**, 1196 (2006), astro-ph/0602306.

[3] J. Wilms et al., Mon. Not. Roy. Astron. Soc. **328**, L27 (2001), astro-ph/0110520.

[4] J.-M. Wang, Y.-M. Chen, L. C. Ho, and R. J. McLure, Astrophys. J. **642**, L111 (2006), astro-ph/0603813.

[5] G. Miniutti, A. C. Fabian, and J. M. Miller, Mon. Not. Roy. Astron. Soc. **351**, 466 (2004), astro-ph/0311037.

[6] S. N. Zhang, W. Cui, and W. Chen, Astrophys. J. **482**, L155 (1997), astro-ph/9704072.

[7] C. S. Reynolds and A. C. Fabian (2007), arXiv:0711.4158 [astro-ph].

[8] F. Pretorius, Phys. Rev. Lett. **95**, 121101 (2005), gr-qc/0507014.

[9] M. Campanelli, C. O. Lousto, P. Marronetti, and Y. Zlochower, Phys. Rev. Lett. **96**, 111101 (2006), gr-qc/0511048.

[10] J. G. Baker, J. Centrella, D.-I. Choi, M. Koppitz, and J. van Meter, Phys. Rev. Lett. **96**, 111102 (2006), gr-qc/0511103.

[11] L. Lindblom, M. A. Scheel, L. E. Kidder, R. Owen, and O. Rinne, Class. Quant. Grav. **23**, S447 (2006), gr-qc/0512093.

[12] C. Gundlach and J. M. Martin-Garcia, Phys. Rev. **D74**, 024016 (2006), gr-qc/0604035.

[13] J. R. van Meter, J. G. Baker, M. Koppitz, and D.-I. Choi, Phys. Rev. **D73**, 124011 (2006), gr-qc/0605030.

[14] M. Campanelli, C. O. Lousto, and Y. Zlochower, Phys. Rev. D **74**, 041501(R) (2006), gr-qc/0604012.

[15] M. Campanelli, C. O. Lousto, and Y. Zlochower, Phys. Rev. D **74**, 084023 (2006), astro-ph/0608275.

[16] M. Campanelli, C. O. Lousto, Y. Zlochower, B. Krish-

nan, and D. Merritt, Phys. Rev. **D75**, 064030 (2007), gr-qc/0612076.

[17] L. Rezzolla et al., Astrophys. J. **674**, L29 (2008), arXiv:0710.3345 [gr-qc].

[18] U. Sperhake et al. (2007), arXiv:0710.3823 [gr-qc].

[19] A. Ashtekar, S. Fairhurst, and B. Krishnan, Phys. Rev. **D62**, 104025 (2000), gr-qc/0005083.

[20] O. Dreyer, B. Krishnan, D. Shoemaker, and E. Schnetter, Phys. Rev. **D67**, 024018 (2003), gr-qc/0206008.

[21] E. Schnetter, B. Krishnan, and F. Beyer, Phys. Rev. **D74**, 024028 (2006), gr-qc/0604015.

[22] B. Krishnan, C. O. Lousto, and Y. Zlochower, Phys. Rev. **D76**, 081501 (2007), arXiv:0707.0876 [gr-qc].

[23] Y. Pan et al., Phys. Rev. **D77**, 024014 (2008), arXiv:0704.1964 [gr-qc].

[24] M. Boyle et al., Phys. Rev. **D76**, 124038 (2007), arXiv:0710.0158 [gr-qc].

[25] M. Hannam, S. Husa, U. Sperhake, B. Brugmann, and J. A. Gonzalez, Phys. Rev. **D77**, 044020 (2008), 0706.1305.

[26] P. Ajith et al., Phys. Rev. **D77**, 104017 (2008), 0710.2335.

[27] M. Campanelli, C. O. Lousto, and Y. Zlochower, Phys. Rev. D **77**, 101501(R) (2008), 0710.0879.

[28] C. O. Lousto and Y. Zlochower, Phys. Rev. **D77**, 024034 (2008), arXiv:0711.1165 [gr-qc].

[29] M. Shibata and K. Uryu, Class. Quant. Grav. **24**, S125 (2007), astro-ph/0611522.

[30] M. Shibata and K. Uryu, Phys. Rev. **D74**, 121503 (2006), gr-qc/0612142.

[31] M. Shibata and K. Taniguchi, Phys. Rev. **D77**, 084015 (2008), 0711.1410.

[32] Z. B. Etienne, J. A. Faber, Y. T. Liu, S. L. Shapiro, K. Taniguchi, and T. W. Baumgarte, Phys. Rev. D **77**,

084002 (2008), arXiv:0712.2460 [astro-ph].

[33] M. Campanelli, C. O. Lousto, Y. Zlochower, and D. Merritt, Astrophys. J. **659**, L5 (2007), gr-qc/0701164.

[34] J. A. González, M. D. Hannam, U. Sperhake, B. Brugmann, and S. Husa, Phys. Rev. Lett. **98**, 231101 (2007), gr-qc/0702052.

[35] M. Campanelli, C. O. Lousto, Y. Zlochower, and D. Merritt, Phys. Rev. Lett. **98**, 231102 (2007), gr-qc/0702133.

[36] F. Herrmann, I. Hinder, D. Shoemaker, P. Laguna, and R. A. Matzner, Astrophys. J. **661**, 430 (2007), gr-qc/0701143.

[37] M. Koppitz et al., Phys. Rev. Lett. **99**, 041102 (2007), gr-qc/0701163.

[38] F. Herrmann, D. Shoemaker, and P. Laguna, AIP Conf. **873**, 89 (2006), gr-qc/0601026.

[39] J. G. Baker et al., Astrophys. J. **653**, L93 (2006), astro-ph/0603204.

[40] J. A. González, U. Sperhake, B. Brugmann, M. Hannam, and S. Husa, Phys. Rev. Lett. **98**, 091101 (2007), gr-qc/0610154.

[41] T. Bogdanovic, C. S. Reynolds, and M. C. Miller (2007), astro-ph/0703054.

[42] A. Loeb, Phys. Rev. Lett. **99**, 041103 (2007), astro-ph/0703722.

[43] E. W. Bonning, G. A. Shields, and S. Salviander (2007), arXiv:0705.4263 [astro-ph].

[44] K. Holley-Bockelmann, K. Gultekin, D. Shoemaker, and N. Yunes (0700), arXiv:0707.1334 [astro-ph].

[45] F. Herrmann, I. Hinder, D. M. Shoemaker, P. Laguna, and R. A. Matzner, Phys. Rev. **D76**, 084032 (2007), arXiv:0706.2541 [gr-qc].

[46] B. Brugmann, J. A. Gonzalez, M. Hannam, S. Husa, and U. Sperhake, Phys. Rev. **D77**, 124047 (2008), 0707.0135.

[47] S. Komossa, H. Zhou, and H. Lu, Astrop. J. Letters **678**, L81 (2008), 0804.4585.

[48] W. Tichy, B. Brügmann, M. Campanelli, and P. Diener, Phys. Rev. D **67**, 064008 (2003), gr-qc/0207011.

[49] B. J. Kelly, W. Tichy, M. Campanelli, and B. F. Whiting, Phys. Rev. **D76**, 024008 (2007), 0704.0628.

[50] S. Dain, C. O. Lousto, and R. Takahashi, Phys. Rev. D **65**, 104038 (2002), gr-qc/0201062.

[51] G. Cook and J. W. York, Phys. Rev. D **41**, 1077 (1990).

[52] J. Baker, M. Campanelli, C. O. Lousto, and R. Takahashi, Phys. Rev. D **69**, 027505 (2004).

[53] L. Rezzolla et al., Astrophys. J. **679**, 1422 (2008), arXiv:0708.3999 [gr-qc].

[54] A. Buonanno, L. E. Kidder, and L. Lehner, Phys. Rev. **D77**, 026004 (2008), arXiv:0709.3839 [astro-ph].

[55] L. Rezzolla et al. (2007), arXiv:0712.3541 [gr-qc].

[56] M. C. Washik et al. (2008), arXiv:0802.2520 [gr-qc].

[57] I. Hinder, B. Vaishnav, F. Herrmann, D. Shoemaker, and P. Laguna, Phys. Rev. **D77**, 081502 (2008), 0710.5167.

[58] J. M. Bowen and J. W. York, Jr., Phys. Rev. D **21**, 2047 (1980).

[59] R. Bartnik and J. Isenberg, in *The Einstein equations and large scale behavior of gravitational fields*, edited by P. T. Chruściel and H. Friedrich (Birhäuser Verlag, Basel Boston Berlin, 2004), pp. 1–38, gr-qc/0405092.

[60] S. Brandt and B. Brügmann, Phys. Rev. Lett. **78**, 3606 (1997), gr-qc/9703066.

[61] S. Dain, Phys. Rev. Lett. **96**, 101101 (2006), ISSN 0031-9007, gr-qc/0511101.

[62] S. Dain (2006), to appear in J. Differential Geometry, gr-qc/0606105.

[63] M. W. Choptuik, Ph.D. thesis, University of British Columbia (1986).

[64] S. Dain and M. E. G. Clement (2008), 0806.2180.

[65] G. A. Avila and S. Dain (2008), 0805.2754.

[66] S. R. Brandt and E. Seidel, Phys. Rev. **D54**, 1403 (1996), gr-qc/9601010.

[67] Cactus Computational Toolkit home page: http://www.cactuscode.org.

[68] G. B. Cook and J. York, James W., Phys. Rev. **D41**, 1077 (1990).

[69] J. Baker, M. Campanelli, and C. O. Lousto, Phys. Rev. D **65**, 044001 (2002), gr-qc/0104063.

[70] M. Campanelli, C. O. Lousto, and Y. Zlochower, Phys. Rev. D **73**, 061501(R) (2006).

[71] M. Ansorg, B. Brügmann, and W. Tichy, Phys. Rev. D **70**, 064011 (2004), gr-qc/0404056.

[72] Y. Zlochower, J. G. Baker, M. Campanelli, and C. O. Lousto, Phys. Rev. D **72**, 024021 (2005), gr-qc/0505055.

[73] T. Nakamura, K. Oohara, and Y. Kojima, Prog. Theor. Phys. Suppl. **90**, 1 (1987).

[74] M. Shibata and T. Nakamura, Phys. Rev. D **52**, 5428 (1995).

[75] T. W. Baumgarte and S. L. Shapiro, Phys. Rev. D **59**, 024007 (1999), gr-qc/9810065.

[76] E. Schnetter, S. H. Hawley, and I. Hawke, Class. Quantum Grav. **21**, 1465 (2004), gr-qc/0310042.

[77] M. Alcubierre, B. Brügmann, P. Diener, M. Koppitz, D. Pollney, E. Seidel, and R. Takahashi, Phys. Rev. D **67**, 084023 (2003), gr-qc/0206072.

[78] B. Bruegmann et al. (2006), gr-qc/0610128.

[79] J. Thornburg, Class. Quantum Grav. **21**, 743 (2004), gr-qc/0306056.

[80] O. Dreyer, B. Krishnan, D. Shoemaker, and E. Schnetter, Phys. Rev. D **67**, 024018 (2003), gr-qc/0206008.

[81] M. Campanelli and C. O. Lousto, Phys. Rev. D **59**, 124022 (1999), gr-qc/9811019.

[82] C. O. Lousto and Y. Zlochower, Phys. Rev. D **76**, 041502(R) (2007), gr-qc/0703061.

[83] C. O. Lousto and Y. Zlochower, Phys. Rev. **D77**, 044028 (2008), arXiv:0708.4048 [gr-qc].

[84] M. Hannam, S. Husa, B. Brugmann, and A. Gopakumar (2007), arXiv:0712.3787 [gr-qc].

[85] F. Echeverría, Phys. Rev. D **40**, 3194 (1989).

[86] J. G. Baker, M. Campanelli, C. O. Lousto, and R. Takahashi, Phys. Rev. **D69**, 027505 (2004), astro-ph/0305287.

[87] M. Hannam, S. Husa, D. Pollney, B. Brugmann, and N. O'Murchadha, Phys. Rev. Lett. **99**, 241102 (2007), gr-qc/0606099.

[88] T. W. Baumgarte and S. G. Naculich, Phys. Rev. **D75**, 067502 (2007), gr-qc/0701037.

[89] J. D. Brown (2007), arXiv:0705.1359 [gr-qc].

[90] M. Hannam, S. Husa, F. Ohme, B. Brugmann, and N. O'Murchadha (2008), 0804.0628.

[91] G. Lovelace, R. Owen, H. P. Pfeiffer, and T. Chu (2008), 0805.4192.

[92] An alternative method for generating highly-spinning binaries, which was released as a preprint a few months after this paper was submitted, is given in [91]